Electrostatic Complementarity Drives Amyloid/Nucleic Acid Co-assembly

Allisandra K. Rha, Dibyendu Das, Anil K. Mehta, Olga Taran, Yonggang Ke, and David G. Lynn*

*To whom correspondence should be addressed: dlynn2@emory.edu

This file includes:
Supplementary Figures 1-9
Corresponding materials and methods

Table of Contents

Peptide Assembly

Peptide/RNA Co-assembly

Solid State NMR

Supplementary Experimental Details

Peptide Assembly

Methods

Peptide Synthesis

Peptides were synthesized using Solid Phase Peptide Synthesis with microwave synthesis (CEM, Matthews, NC, USA) with FMOC-protected natural abundance (Anaspec, Fremont, CA) amino acids on a Rink-Amide MBHA resin, 0.4mmol/g substitution, and capped at the N-terminus with an acetyl group. Peptides were cleaved and deprotected using a cocktail of 90% TFA, 2% anisole, 3% 1,2-ethanedithiol, and 5% thioanisole. All chemicals were purchased from Sigma-Aldrich. Following cleavage and deprotection, peptides were purified by reverse-phase HPLC using acetonitrile and water with 0.1%TFA and a Waters Atlantis C18 column to >98% purity. After purification, acetonitrile was removed *in vacuo*. The remaining aqueous solution was frozen at -80°C or flash frozen using liquid nitrogen and lyophilized to yield a white powder.

Peptide Assembly

Due to the salt sensitivity of peptides and nucleic acids during assembly in this study, following purification and lyophilization, peptides were desalted using Sep-Pak® C18 cartridges (Waters). The resulting solutions were flash frozen using liquid nitrogen or overnight at -80C, lyophilized to yield a white powder, and concentrations determined from the dry weight of these lyophilized powders. Peptides were dissolved in 40% Acetonitrile with brief vortexing and then sonicated for 5 minutes. The pH was not adjusted and the pH each sample was measured to be pH5. A stock solution of 2mM peptide was used for all peptide assemblies. Samples were set up within five minutes of dissolution. For Nucleic acid/Peptide co-assemblies, a stock solution of 1mM nucleic acids (Integrated DNA Technologies) was used. Order of addition was as follows: Peptide, solvent, nucleic acid. Assemblies were kept at 4°C unless otherwise noted. Final peptide concentration in all experimental setups was 1mM. Final nucleic acid concentration depended on length. All co-assemblies were established with a 1:1 (peptide:nucleic acid) charge ratio.

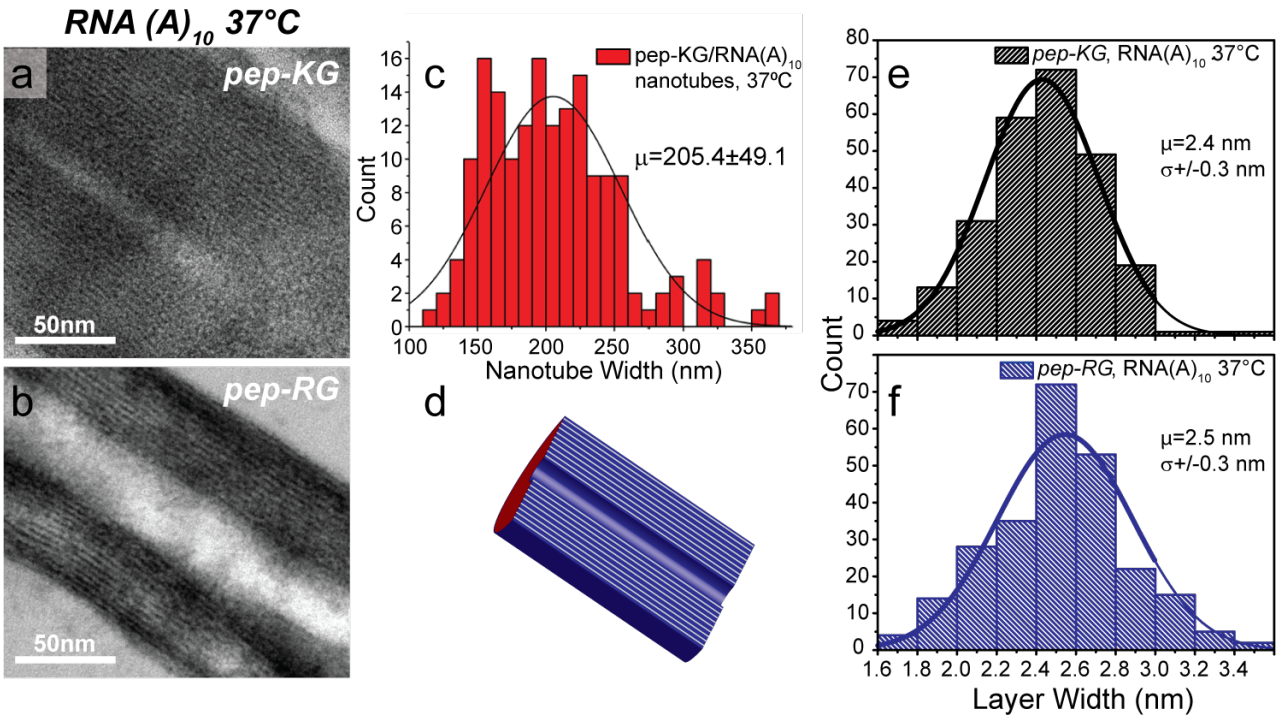

Supplementary Figure 1. Characterization of multi-lamellar peptide/RNA nanotubes. Transmission electron micrographs of nanotube longitudinal cross-sections show multi-lamellar tube walls (a, b). Cross-sections of thick-walled multi-lamellar pep-KG/RNA nanotubes (a, inset). Measurements of nanotube diameter from cross-sections of pep-KG/RNA$(A)_{10}$ co-assemblies at 37°C is 205.4 ± 49.1nm, n=150 (c). Simplified model of multi-lamellar nanotube longitudinal cross-section (d). Measurements of individual lamella within the tube walls define each lamella as 2.4±0.3nm and 2.5±0.3nm for pep-KG/RNA and pep-RG/RNA co-assemblies, respectively (e, f).

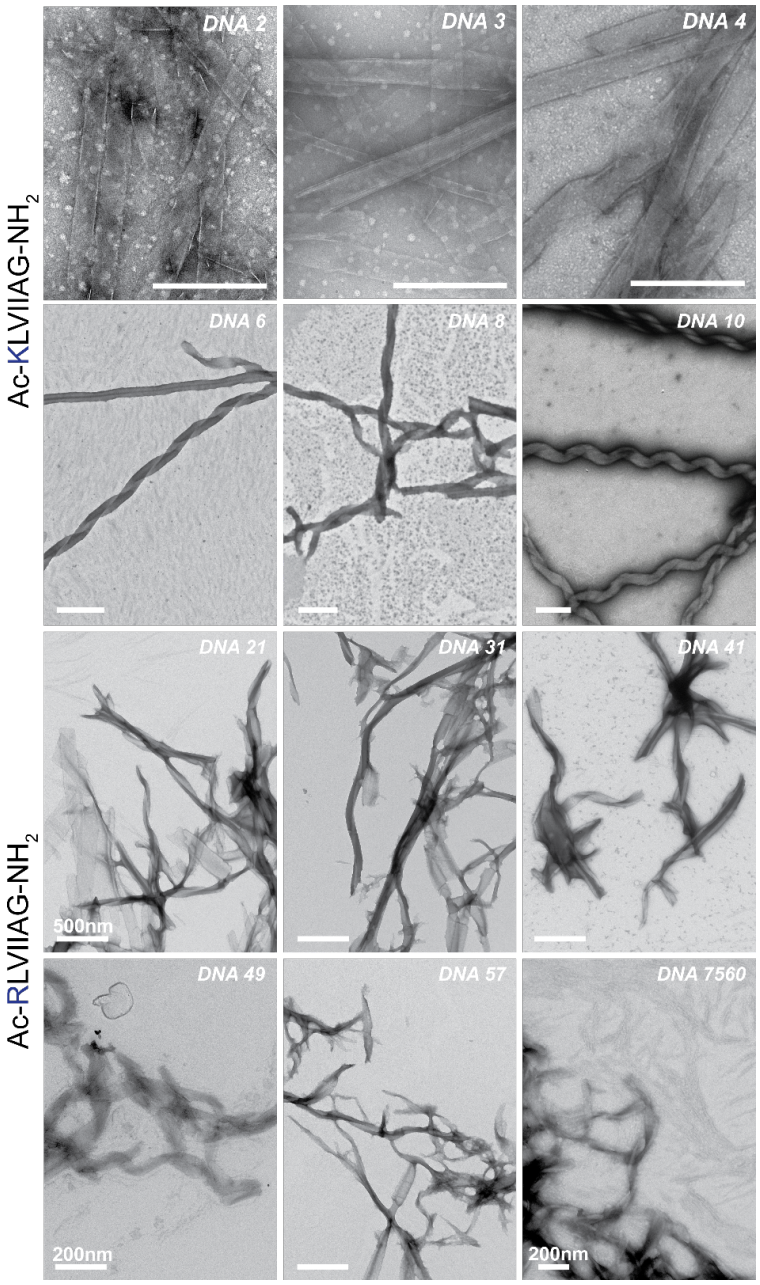

Supplementary Figure 2. Assessment of varying DNA strand length on overall co-assembly morphology and homogeneity. Transmission electron micrographs of *pep-KG* (Ac-KLVIIAG-NH_2) and *pep-RG* (Ac-RLVIIAG-NH_2) co-assembled with DNA(A) from 2 nucleotides to 7560 nucleotides. A minimum strand length of six nucleotides was necessary to achieve ribbonous assemblies. DNA with a strand length of 10 nucleotides gave the most homogeneous assemblies. DNA strand lengths of at least 7560 nucleotides yielded ribbon co-assemblies. Heterogeneity in co-assemblies is attributed to DNA prep when sheets are observed ($d(A)_{21}$), and to an unmatched charge distribution in all other cases. Thinner ribbons are observed in several cases, but the overall morphology appears similar. Scale bars are 500nm unless otherwise noted.

Laser Scanning Confocal Microscopy

Fluorescence micrographs were obtained using an Olympus FluoView 1000 (FV1000) laser-scanning confocal microscope. Thioflavin T was added to samples at a final concentration of 2mM prior to placement on microscope slides, with coverslips sealed using clear nail polish and examined using a 60X 1.42NA oil immersion objective using 405nm laser line. RNA$(A)_{10}$ with Cy3 covalently attached at the 3'-end was purchased from Integrated DNA Technologies and visualized using a 559nm laser line. Images for Thioflavin T and Cy3 fields were obtained concurrently and processed using Fiji image analysis software[1].

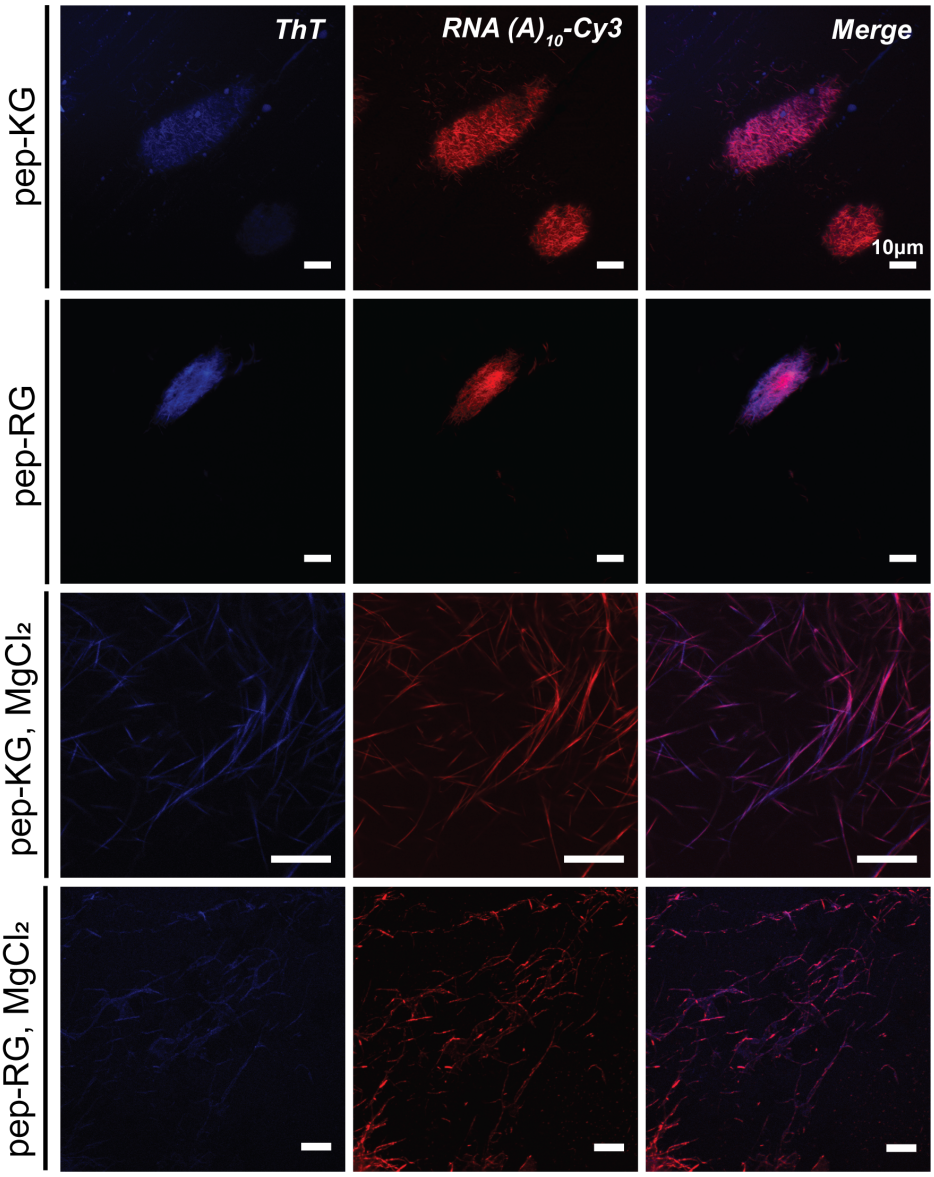

Supplementary Figure 3. RNA/Peptide co-assembly visualized by laser scanning confocal microscopy. *Pep-KG* and *pep-RG* co-assembled with RNA$(A)_{10}$-Cy3 at 4°C, rows one and two, respectively. *Pep-KG* and *pep-RG* co-assembled with RNA$(A)_{10}$-Cy3 in the presence of 300mM $MgCl_2$, rows three and four, respectively. For all assemblies, fluorescence of ThioflavinT (ThT), an amyloid specific dye, is shown in the left panel, Cy3 covalently attached to RNA at the 3'-end in the middle panel, and the merge of the fluorescence for the two fluorophores in the right panel. Scale bars are 10μm.

Electrostatic Force Microscopy (EFM)

A Park System XE-100 AFM (Suwon 16229, Korea) with a charge bias of +1V applied between the cantilever and the sample created an electrostatic field allowing for the surveying of charge on the assembly surface. Pt-Ir coated cantilevers that are electrically conductive were used in non-contact mode to map electrical properties on the sample surface. The cantilever tip radius was <20nm and had a force constant of 2.8 N/m. Prior to EFM imaging, the NA/Peptide samples were deposited on gold film, Si/SiO_2 substrates. The thickness of the oxide layer was 300nm. The co-assemblies were deposited as 1 µL droplets and dried over 12 hours before examination.

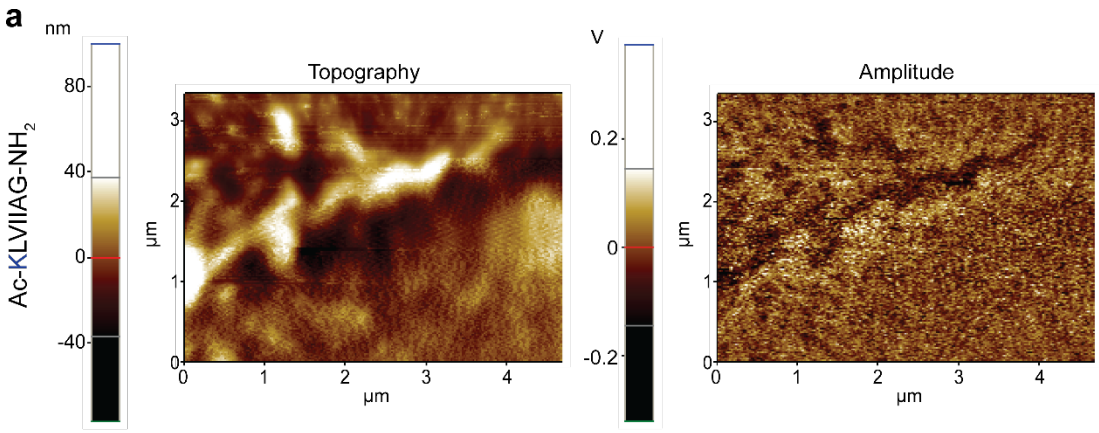

Supplementary Figure 4. Electrostatic Force Micrographs of a *pep-KG*/RNA ribbon. Topography is shown in the left panel with height in nm. Measure of charge distribution is shown in the right panel with dark areas indicating negative surface charge.

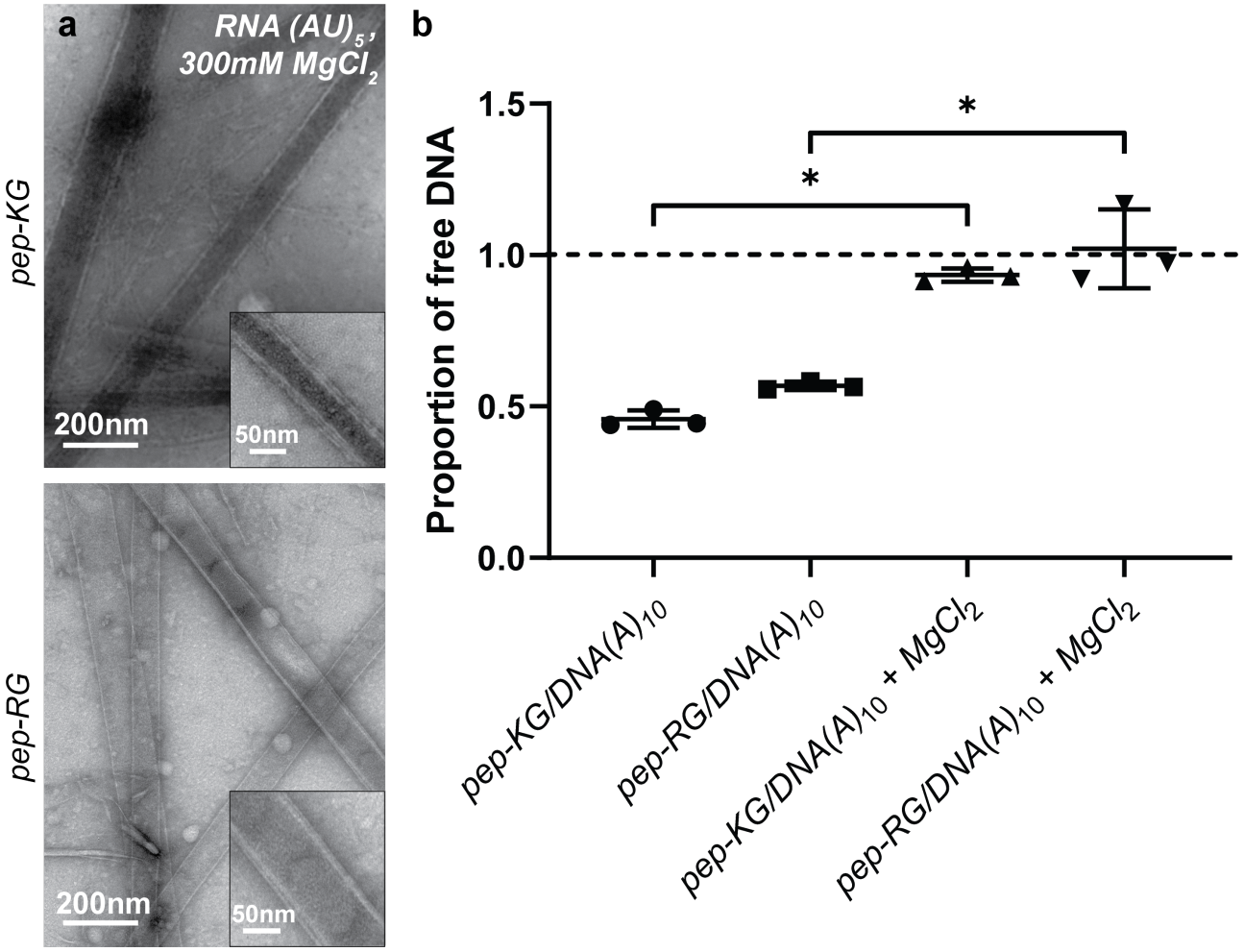

Supplementary Figure 5. Magnesium ion influence on nucleic acid/peptide co-assembly. Transmission electron micrographs of pep-KG/RNA and pep-RG/RNA co-assemblies in the presence of 300mM $MgCl_2$ (a). Nanotube walls have multiple lamellae (insets, a). Measurement of free DNA in supernatant of spun down co-assemblies with and without 300mM $MgCl_2$ (b). *$p<0.05$ Welch's t-test. Dotted line represents total starting DNA. Sample values were measured as absorbance and normalized to starting DNA concentration.

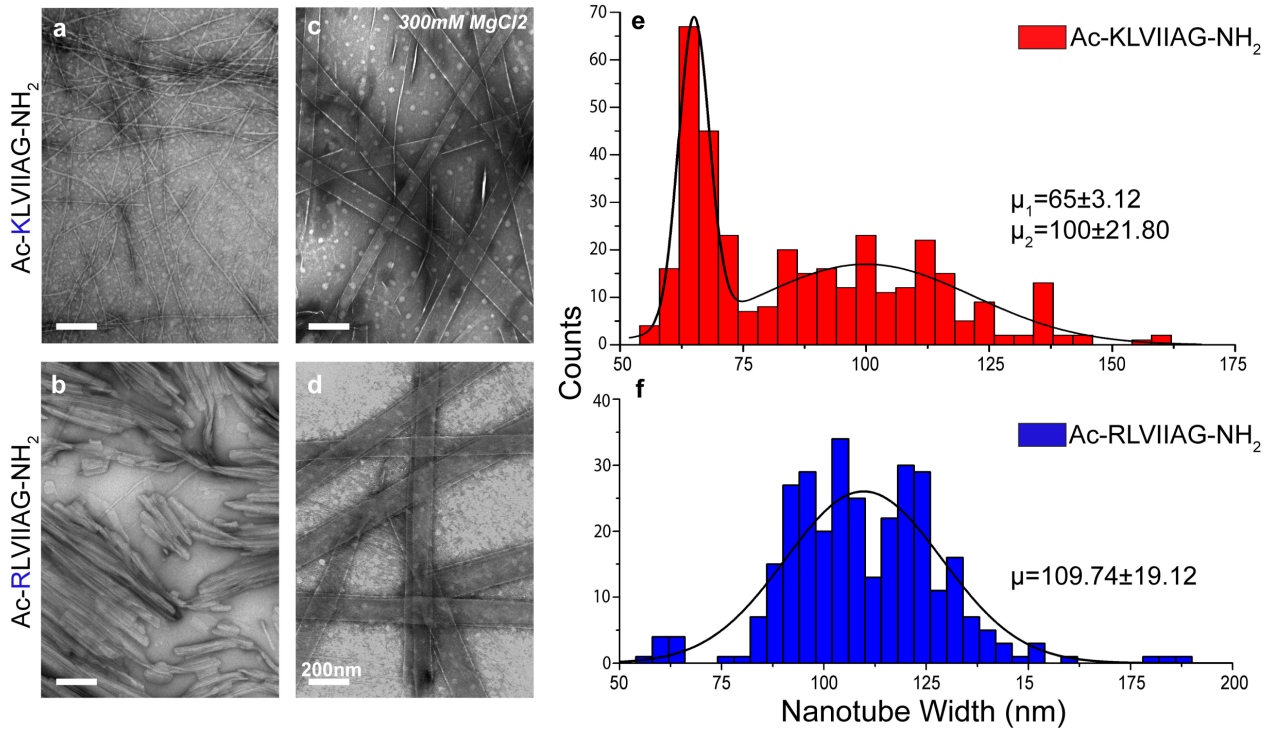

Supplementary Figure 6. Magnesium ion influence on peptide assembly. Transmission electron micrographs of pep-KG and pep-RG assemblies in the absence of $MgCl_2$ (a, b). Pep-KG and pep-RG assemblies in the presence of 300mM $MgCl_2$ (c, d). Measurement of nanotube width for pep-KG and pep-RG assemblies in the presence of 300mM $MgCl_2$ (e, f). For pep-KG assemblies, two nanotube populations were measured with mean widths of 65±3.12 and 100±21.80nm. Pep-RG nanotubes had a mean width of 109.74±19.12nm. All scale bars are 200nm.

Synthesis of $Zr[(O_3PCH_2)(HO_3PCH_2)NHCH_2COOH]_2 \cdot 2H_2O$ as a $^{13}C\{^{31}P\}$REDOR Calibration Standard

$Zr[(O_3PCH_2)(HO_3PCH_2)NHCH_2COOH]_2 \cdot 2H_2O$ (**Supplementary Fig. 7**) was synthesized following literature protocol[2]. A clear solution of (2-^{13}C) Glyphosine (300mg, 1.2mmol, Cambridge Isotopes, Tewksbury, MA) in 9mL of water was added to a solution of $ZrOCl_2 \cdot 8H_2O$ (192mg, 0.6mmol) in 2.9M HF (2.46mL, 7.2mmol) in a closed HDPE vessel. The mixture was maintained at 80°C for 7 days in a mineral oil bath. White crystals were obtained and isolated using vacuum filtration. After washing with water, crystals were placed in a vacuum desiccator where they were dried for 48 hours. A 97mg quantity of product was recovered. The product was confirmed to be the correct structure by XRD with unit cell dimensions as follows: a = 5.44Å, b = 14.95Å, c = 13.31Å, α = 90°, β = 95.26°, γ = 90°.

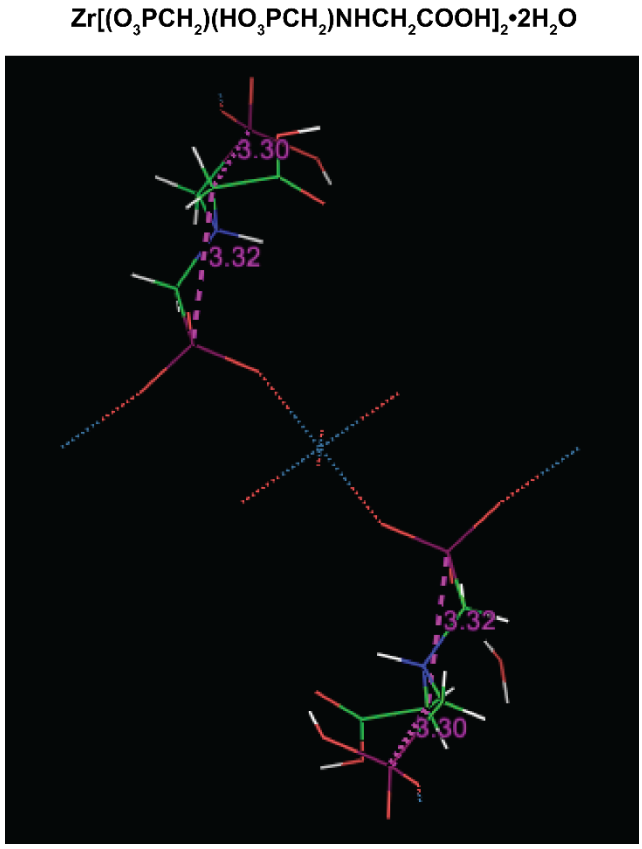

Supplementary Figure 7. Structure rendered from CSD RISJEK[1]. Measurements indicate distances between phosphorus nuclei and ^{13}C-enriched carbon. Only distances within 5Å are shown.

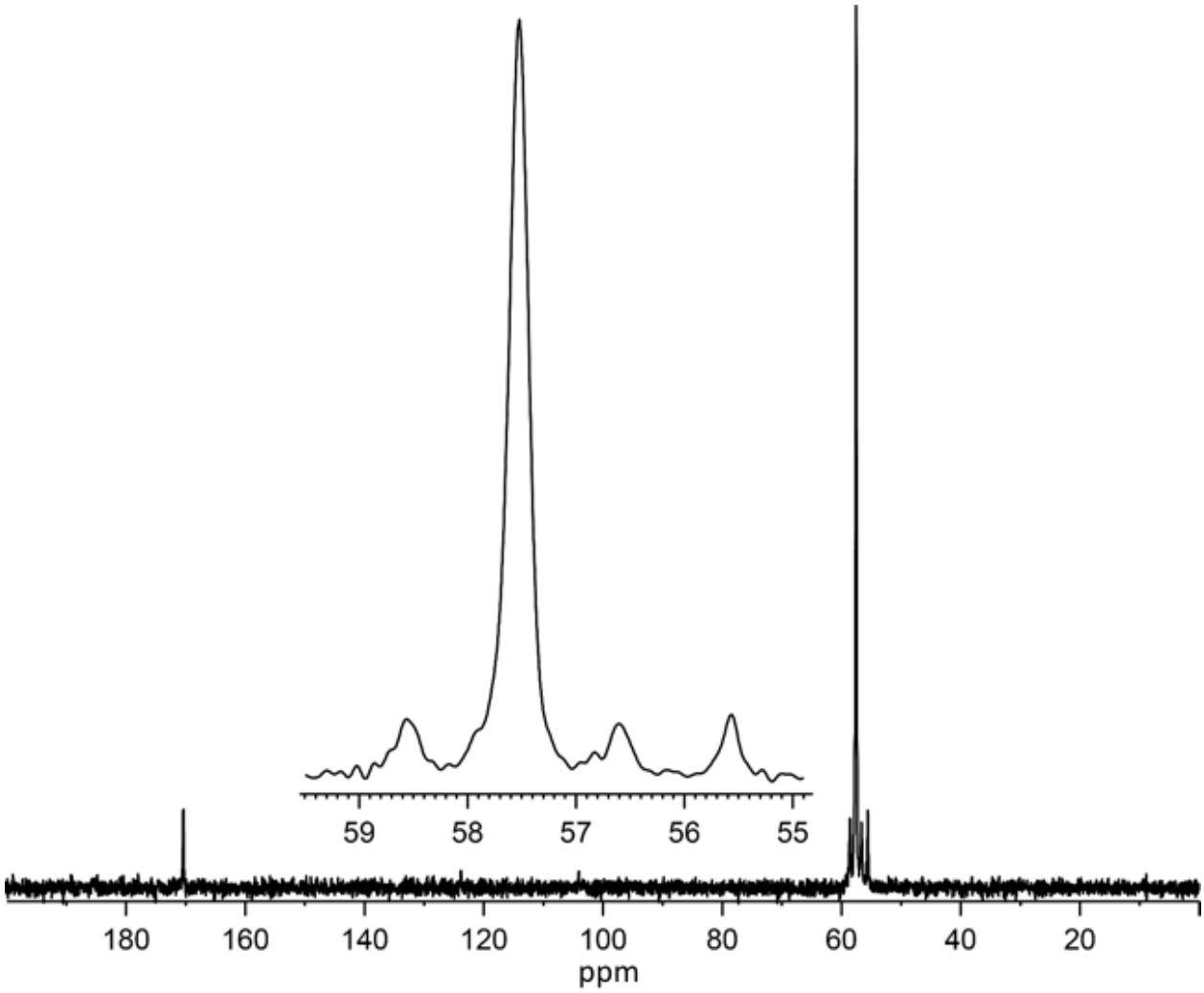

Supplementary Figure 8. Solid-state ^{13}C (150.928 MHz) NMR spectrum of $Zr[(O_3PCH_2)(HO_3PCH_2)NHCH_2COOH]_2 \cdot 2H_2O$.

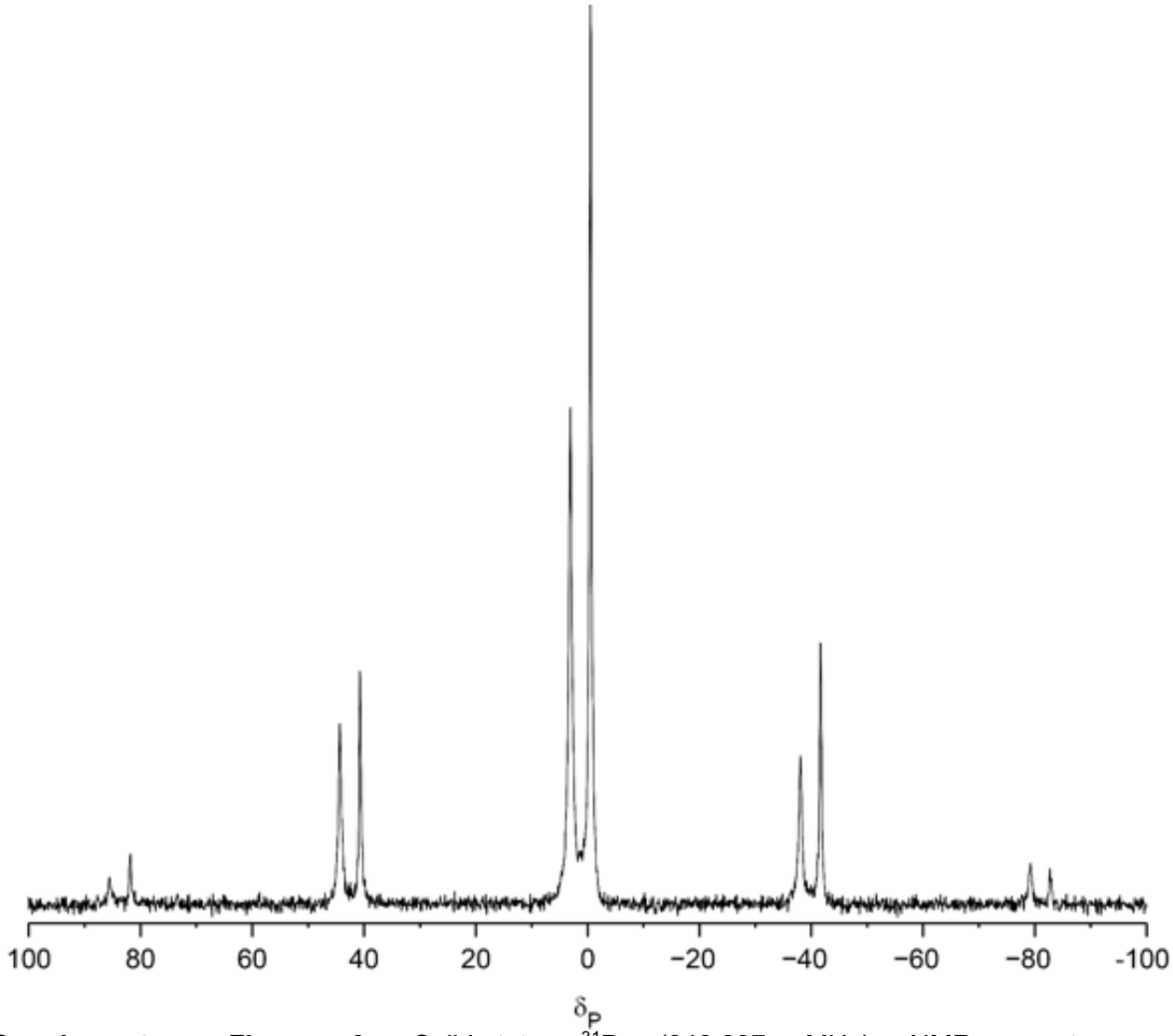

Supplementary Figure 9. Solid-state ^{31}P (242.937 MHz) NMR spectrum of $Zr[(O_3PCH_2)(HO_3PCH_2)NHCH_2COOH]_2 \cdot 2H_2O$. All phosphorus nuclei exist in the same environment.

Solid-State NMR

Pep-KG was synthesized via Solid Phase Peptide Synthesis (SPPS) with isotopically enriched [1-^{13}C]Leucine and [^{15}N]Alanine (Cambridge Isotopes) and assembled with nucleic acid templates at room temperature. A Bruker Avance 600mHz solid-state NMR spectrometer with a Bruker 4mm HCN BioSolids magic-angle spinning (MAS) probe was used to collect NMR spectra. ^{13}C CP-MAS spectra before and after REDOR and ^{13}C DQF-DRAWS experiments, confirmed the sample did not degrade during the experiment. Samples were centered in 4mm MAS ceramic rotors with

boron nitride spacers. All spectra were collected with spin-temperature alternation of the initial ^{1}H (600.133 MHz) 1.9μs $\pi/2$ pulse. ^{1}H cross-polarization RF fields were ramped from 50 to 70 kHz and the ^{13}C (150.929 MHz) cross-polarization RF field was kept constant at 50kHz. SPINAL-64 ^{1}H decoupling at 128 kHz was used during both dipolar evolution and acquisition.

During the REDOR experiments, MAS frequency was actively maintained at 10kHz +/- 2 Hz with exit cooling and spinning air temperature below -1°C, to prevent sample denaturation. The $^{13}C\{^{15}N\}$REDOR[3] pulse sequence[4] consists of two parts, an S sequence that contains both ^{13}C (150.928 MHz) and ^{15}N (60.818 MHz) rotor synchronized xy8 phase cycled[5] π-pulses of 4μs and 8μs respectively, and a full-echo (S_0) sequence which is identical but does not contain any ^{15}N dephasing pulses. In addition to xy8 phase cycling of the REDOR π-pulses, the last refocusing π-pulse followed exorcycle phase cycling[6] to minimizing the effects of RF inhomogeneity. The $^{13}C\{^{31}P\}$REDOR pulse sequences were identical with 10μs ^{31}P π-pulses. REDOR data points are the integrated sum of center- and sideband peaks. Error bars are calculated using the noise of each spectrum as the maximum peak height deviation. To normalize for the decay due to T_2 (spin-spin relaxation), individual REDOR curves are plotted as $\Delta S/S_0$. The REDOR dephasing curves is directly related to the ^{13}C-^{15}N or ^{13}C-^{31}P dipolar coupling, in the $^{13}C\{^{15}N\}$REDOR and $^{13}C\{^{31}P\}$REDOR experiments, respectively, hence the distance between the spins. As more than one ^{15}N and ^{31}P is present, the resulting REDOR curves depends on both the ^{13}C-$^{15}N/^{31}P$ distances as well as the relative orientations of the ^{13}C-$^{15}N/^{31}P$ internuclear vectors[7], [8]. The effects of finite pulses on REDOR dephasing was calibrated with [1-^{13}C,^{15}N]Alanine diluted 10:1[9] for $^{13}C\{^{15}N\}$REDOR and with $Zr[(O_3PCH_2)(HO_3PCH_2)NHCH_2COOH]_2 \cdot 2H_2O$ as described below for $^{13}C\{^{31}P\}$REDOR..

^{13}C DQF-DRAWS experiments were implemented with phase cycling previously described[10] and 41.23 kHz ^{13}C RF field for DRAWS pulses, measured by fitting a ^{13}C nutation curve to a sine function with a decaying exponential. The rotor period (206.2μs $\rightarrow$ ν_r= 4.85 kHz) was set to 8.5 times the ^{13}C π pulse length. T_2DQ = 11.2 ms was measured in separate experiments by placing a composite 90x-90y-90x DQ coherence refocusing pulse[11] between the two DRAWS evolution periods which were fixed at 40-Tr. Data points are the ratio of the sum of center- and sideband-integrated peak intensities for each evolution time to the ^{13}C CP-MAS intensities. Error bars are calculated using the noise of each spectrum as the maximum peak height deviation. DQF-DRAWS curves were calculated using SIMPSON[12], where an array of ^{13}C spins were approximated with an “infinite-loop” model[11] and chemical shift tensor components δ_{11}=74.1ppm, δ_{22}=6.0ppm and δ_{33}=-80.1p pm, which were measured from the ^{13}C CP-MAS

spectra. The infinite loop model consists of three spins with identical dipolar couplings but with the orientation of the CSA to dipolar tensors identical between spins 1-2 and spins 3-1. The effects of DQ-relaxation were approximated by multiplying the calculated SQ intensity with a decaying exponential of the form $e^{-\frac{t}{2*T_2DQ}}$ with T_2DQ = 11.2 ms. DRAWS curves were calculated from 3Å to 7Å and used to find a best fit to the experimental data points by minimizing the residual: $\chi = \sqrt{\frac{\sum_{i=1}^{n} w_i(x_i - x_{\mathrm{calc}})^2}{n}}$, where x_i and w_i are the experimental data and error, respectively.

$^{13}C\{^{31}P\}$REDOR of $Zr[(O_3PCH_2)(HO_3PCH_2)NHCH_2COOH]_2 \cdot 2H_2O$

$^{13}C\{^{31}P\}$REDOR was carried out as described in the main text. All ^{31}P nuclei within 10Å of [2-^{13}C] Glyphosine of $Zr[(O_3PCH_2)(HO_3PCH_2)NHCH_2COOH]_2$ contributed to ^{13}C-^{31}P dephasing and were included in the calculations. Knowledge of all the ^{13}C and ^{31}P nuclei positions from the crystal structure of this sample allowed for its use as a standard for ^{13}C – ^{31}P distance measurements.

References

[1] J. Schindelin *et al.*, *Nat. Methods* **2012**, *9*, 676–682.

[2] M. Taddei, A. Donnadio, F. Costantino, R. Vivani, and M. Casciola, *Inorg. Chem* **2013**, *52*, 12131–12139.

[3] T. Gullion in *Modern Magnetic Resonance*, (Dordrecht) Springer, Netherlands, **2008**, pp. 713–718.

[4] A. M. Christensen and J. Schaefer, *Biochemistry* **1993**, *32*, 2868–2873.

[5] T. Gullion, D. B. Baker, and M. S. Conradi, *J. Magn. Reson.* **1990**, *89*, 479–484.

[6] M. Rance and R. A. Byrd, *J. Magn. Reson.* **1983**, *52*, 221-240.

[7] T. P. Jarvie, G. T. Went, and K. T. Mueller, *J. Am. Chem. Soc.* **1996**, *118*, 5330-5331.

[8] J. M. Goetz and J. Schaefer, *J. Magn. Reson.* **1997**, *127*, 147–154.

[9] A. K. Mehta *et al.*, *J. Am. Chem. Soc.* **2008**, *130*, 9829–9835.

[10] M. A. Mehta, M. T. Eddy, S. A. McNeill, F. D. Mills, and J. R. Long, *J. Am. Chem. Soc.* **2008**, *130*, 2202-2212.

[11] D. M. Gregory *et al.*, *Solid State Nucl. Magn. Reson.* **1998**, *13*, 149-166.

[12] M. Bak, J. T. Rasmussen, and N. C. Nielsen, *J. Magn. Reson.* **2000**, *147*, 296–330.